

## Photodouble Ionization Dynamics for Fixed-in-Space H<sub>2</sub>

M. Gisselbrecht,<sup>1</sup> M. Lavollée,<sup>1</sup> A. Huetz,<sup>1</sup> P. Bolognesi,<sup>2</sup> L. Avaldi,<sup>2</sup> D. P. Seecombe,<sup>3</sup> and T. J. Reddish<sup>3</sup>

<sup>1</sup>CNRS, Université Paris-Sud, LIXAM UMR8624, Bâtiment 350, Orsay Cedex, F-91405, France

<sup>2</sup>CNR -IMIP Area della Ricerca di Roma 1, CP 10 00016 Monterotondo Scalo, Italy

<sup>3</sup>Department of Physics, University of Windsor, 401 Sunset Avenue, Ontario, Canada, N9B 3P4

(Received 18 January 2006; published 21 April 2006)

The Coulomb explosion of the hydrogen molecule, after absorption of a 76 eV photon, has been studied by momentum imaging the two electrons and the two protons. Absolute fully differential cross sections of high statistical quality are obtained. A subset of the overall data, namely, equal electron-energy sharing, is used to investigate the effects of molecular orientation on the photoelectron angular distribution. Departures from the first-order heliumlike model are evident in detection geometries where electron-electron correlation is “frozen.”

DOI: [10.1103/PhysRevLett.96.153002](https://doi.org/10.1103/PhysRevLett.96.153002)

PACS numbers: 33.80.Eh, 34.10.+x

During the last decade experimental techniques have been steadily improving, enabling studies of the correlated electron pair dynamics produced in photodouble ionization (PDI). PDI of the simplest two-electron molecule, H<sub>2</sub>, is significantly more complex than the well-studied case of helium and introduces new physical effects. First, there is no unique double ionization threshold; the threshold energy depends on internuclear separation as the upper repulsive potential curve is purely Coulombic. Second, the ground state electronic configuration is inevitably more complex as a result of the two-center nuclear potential. Third, PDI in H<sub>2</sub> is followed by a so-called “Coulomb explosion” as the two protons rapidly separate in opposite directions. Since the photo-fragmentation process is rapid compared to molecular rotation, the relative momentum of the two escaping protons defines the molecular alignment at the instant of double ionization. Energy- and angle-resolved detection of all four particles—with a well-defined light polarization state—completely defines the PDI dynamics and allows one to study fully differential cross sections (FDCS) within the *molecular* frame using such “fixed-in-space” molecules. These measurements provide the most stringent tests for theory and the greatest possible physical insight into this prototypical 4-body process.

Experiments of this type on molecular hydrogen (D<sub>2</sub>) have recently become feasible [1,2]. In this study we report on such measurements performed on H<sub>2</sub> at the Elettra 3rd generation synchrotron source operated in the four bunch mode, and using the CIEL momentum imaging apparatus [3,4]. The two electrons and two protons from the Coulomb explosion of H<sub>2</sub> molecules were detected with 4 $\pi$  sr detection efficiency. Approximately  $1.1 \times 10^6$  four-particle coincidence events were obtained, resulting in significantly improved data quality and a clearer understanding of this fundamental process.

Our momentum imaging apparatus [3,4] is based on the same principles as that of recent studies [1,2]. Briefly, the CIEL apparatus comprises two coaxial time-of-flight ana-

lyzers, each fitted with a position-sensitive detector with multihit capability [4]. The gaseous H<sub>2</sub> target molecules are ionized by 100% linearly polarized vacuum ultraviolet synchrotron radiation and the resulting charged particles are extracted by a static electric field ( $E = 26 \text{ V cm}^{-1}$ ) applied across the interaction region, the electrons traveling to one side and the ions to the other. An axial magnetic field ( $B = 20 \text{ Gauss}$ ) is also applied to the system, which serves to confine electrons having an initial large orthogonal velocity component. The  $(x, y, t)$  information of *all four* ejected particles are obtained for each double ionization event and directly mapped to corresponding  $(p_x, p_y, p_z)$  components using classical equations of motion [3].

In this work the photon energy was 76.09 eV, 25 eV above the nominal threshold at the equilibrium internuclear separation and near the peak of the double ionization total cross section. The CIEL apparatus was able to detect electrons from 2 to 23 eV in addition to the two  $\sim 10 \text{ eV}$  protons. The angle and relative energy resolutions were typically 5° and 15%, respectively, for 12.5 eV electrons. *Absolute* FDCS were obtained by extending the method reported in [5] and using the integral cross section of 2.5 kBarns at 25 eV above threshold [6].

We present here a subset of the available data and consider only the equal electron-energy sharing case,  $E_1 = E_2 = 12.5 \pm 2.5 \text{ eV}$ . First, we focus on the “coplanar” geometry, where the electron momenta,  $\hat{k}_{1,2}$ , and polarization vector,  $\hat{\epsilon}$ , all lie in the same plane. In the dipole approximation the FDCS have axial symmetry around the polarization axis and reflection symmetry with respect to the plane perpendicular to it. These properties, which are verified in our measurements, can be used to sum equivalent events together, thus improving the statistics. They also allow us to write the FDCS as:  $d\sigma^7/d\theta_1 d\theta_2 d\Delta\phi_{12} d\theta_N d\Delta\phi_{eN} dE_1 dE_2$ , where  $\theta_{1,2,N}$  are the polar angles of electrons 1 and 2 and the molecular axis,  $N$ , with respect to  $\hat{\epsilon}$ , and where  $\Delta\phi_{12} = \phi_1 - \phi_2$  and  $\Delta\phi_{eN} = \phi_e - \phi_N$  (with  $e = 1$  or  $2$ ) are the relative azimuthal angles. For simplicity, only FDCSs for  $\theta_1 = 90^\circ$

and  $0^\circ$  are shown in Figs. 1 and 2, respectively, for a series of “in-plane” molecular axis orientations. A cursory inspection of Figs. 1 and 2 reveals at least three main features.

(i) In Figs. 1(a) and 1(d), corresponding to the  $\Pi$  and  $\Sigma$  orientations, respectively, the FDCSs have a characteristic symmetrical two-lobe structure very similar to that observed in helium with  $E_1 = E_2$  at the same  $\theta_1$  angle. Coulomb repulsion between the electrons is responsible for the overall tendency for the electrons to be in opposite hemispheres, with strict quantum mechanical node in the FDCS for “back-to-back” emission. The two lobes are slightly closer together (i.e., further away from the direction of the reference electron) in Fig. 1(a) than in 1(d), which indicates a greater degree of electron correlation in the case of  $\Pi$  orientation. In Figs. 2(a) and 2(d), all data related by axial symmetry around  $\hat{\epsilon}$  have been added, resulting in only one lobe, but the same variation in angular correlation is observed.

(ii) The electron-electron angular distribution clearly *does* depend on the molecular alignment, as the observed two-lobe patterns become strongly asymmetric in both Figs. 1 and 2 for all  $\theta_N$  angles between the  $\Pi$  and  $\Sigma$

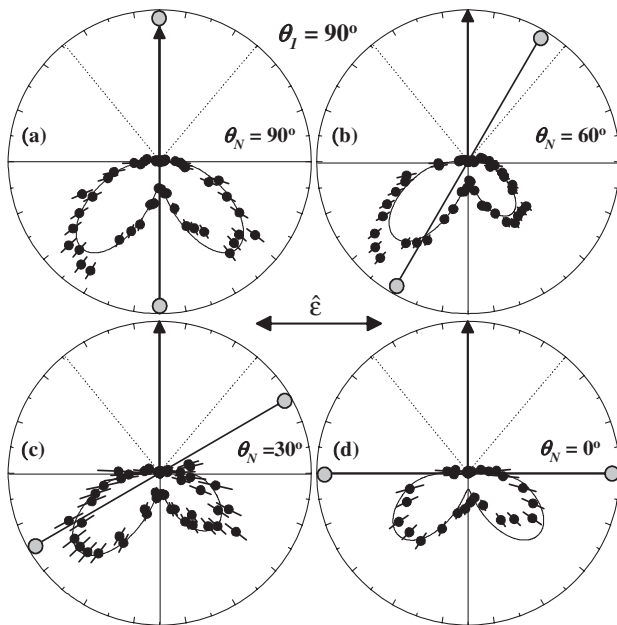


FIG. 1. Absolute  $H_2$  FDCS's in the coplanar geometry ( $|\phi_{12}| = 0^\circ$  or  $180^\circ$ ) for four “in-plane” molecular orientations [ $|\phi_{1N}| = 0^\circ$  or  $180^\circ$ , not relevant in case (d)], as indicated, all with the first electron at  $\theta_1 = 90^\circ$  for  $E_1 = E_2 = 12.5 \pm 2.5$  eV. The radii of the circles give the absolute scales in millibarns/ $eV^2/sr^3$ : 120 (a); 120 (b); 60 (c); 50 (d). The angular step in  $\theta_2$  is  $5^\circ$  (a)–(c) and  $10^\circ$  (d). The dotted lines indicate a small dead sector, symmetric with respect to the first electron, for the detection of the second electron. The angular bandwidths are  $\Delta\theta_1 = \pm 15^\circ$  (a)–(c),  $\pm 20^\circ$  (d);  $\Delta\phi_{12} = \pm 20^\circ$ ;  $\Delta\theta_N = \pm 20^\circ$  (a)–(c),  $\pm 30^\circ$  (d);  $\Delta\phi_{1N} = \pm 45^\circ$ . The full lines give the fit from Eq. (1) folded by experimental bandwidths.

orientations. Within the constraints of electron-electron repulsion, there is a *reduction* in the yield orthogonal to the bond direction.

(iii) The absolute cross section value decreases by about a factor of 4 from  $\Pi$  to  $\Sigma$  orientation. That the ions are not emitted isotropically is well known [7], if not well understood. The improved statistics in the present results allows us to even obtain the FDCS in the pure  $\Sigma$  case.

It is perhaps tempting to regard effects (i) and (ii) as evidence for ion-electron interactions in the final state interpreting the change in lobe peak positions and intensities as due to the electron's Coulomb attraction towards the positive ions. However, this view is probably naive, as it is already well known from PDI studies in atoms that both the initial state of the two active electrons and the interactions in the final state determine the shapes and absolute values of the differential cross sections. Here the two electrons belong primarily to  $\sigma$  orbitals which—due to the molecular orientation—are initially oriented in space and this effect is likely to be important, if not dominant, in the FDCSs measured in the laboratory frame. A better understanding of the observed phenomena clearly requires theoretical investigation.

Feagin and Reddish [8,9] and Kheifets and Bray [10,11] have utilized single-center expansion approaches to this problem with some success, especially for equal energy sharing partially differential cross sections. The general consequences of the optical selection rules for aligned, or

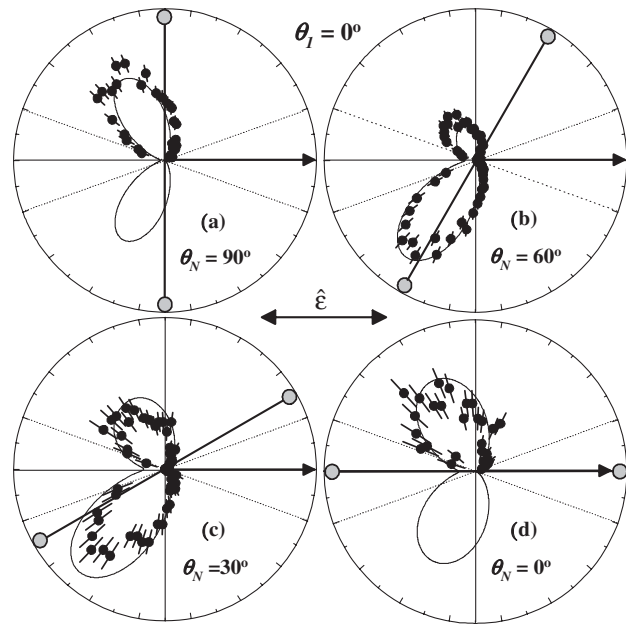


FIG. 2. Same as Fig. 1 but at  $\theta_1 = 0^\circ$ . The angular step in  $\theta_2$  is  $5^\circ$  in all cases. In (a) and (d) only one lobe is reported (see text). The scale in millibarns/ $eV^2/sr^3$  is 40 (a); 50 (b); 30 (c); 20 (d). The coplanar condition for the molecule is  $|\phi_{2N}| = 0^\circ$  or  $180^\circ$ , not relevant in case (d). The angular bandwidths are  $\Delta\theta_1 = \pm 20^\circ$ ;  $\Delta\theta_N = \pm 20^\circ$  (a)–(c),  $\pm 30^\circ$  (d);  $\Delta\phi_{2N} = \pm 45^\circ$ .

“fixed-in-space,”  $H_2$  have been investigated by Briggs and co-workers and elegantly generalized to  $N$ -particle systems [12,13]. In [13] they formally show that Feagin’s heliumlike approach [8,9] is the lowest order approximation in the electron pair angular momentum which is consistent with homonuclear  $H_2$  (or  $D_2$ ). This being the case, we will utilize this model in the work to describe and quantify the main features in the FDCSs.

The form of the fully differential cross section (FDCS) simplifies in the special case where the two electrons have equal energies ( $E_1 = E_2$ ) and is given in this model by:

$$\sigma^{(7)} = \left| \frac{(a_{\Sigma} \cos^2 \theta_N + a_{\Pi} \sin^2 \theta_N)(\cos \theta_1 + \cos \theta_2) + (a_{\Sigma} - a_{\Pi}) \sin \theta_N \cos \theta_N [\sin \theta_1 \cos(\phi_1 - \phi_N) + \sin \theta_2 \cos(\phi_2 - \phi_N)]}{(a_{\Sigma} - a_{\Pi}) \sin \theta_N \cos \theta_N [\sin \theta_1 \cos(\phi_1 - \phi_N) + \sin \theta_2 \cos(\phi_2 - \phi_N)]} \right|^2, \quad (1)$$

where  $a_{\Sigma}$  and  $a_{\Pi}$  are transition amplitudes which depend only on the energies  $E_1$ ,  $E_2$  and the mutual angle  $\theta_{12}$  of the two electrons. They, respectively, account for the PDI process when the molecule is oriented parallel or perpendicular to the polarization axis. For intermediate orientations, the polarization vector  $\hat{\epsilon}$  has two components  $\hat{\epsilon}_{\Sigma}$  and  $\hat{\epsilon}_{\Pi}$  in the molecular frame, respectively, parallel and perpendicular to the internuclear axis, and the two  $\Sigma$  and  $\Pi$  terms are mixed coherently, with coefficients coming from frame transformation and depending only on the angles  $\theta_N$ ,  $\phi_N$ . For  $\theta_N = 0^\circ, 90^\circ$  Eq. (1) reduces to  $|a_{\Sigma}(\cos \theta_1 + \cos \theta_2)|^2$  and  $|a_{\Pi}(\cos \theta_1 + \cos \theta_2)|^2$ , respectively, corresponding to pure  $\Sigma$  and  $\Pi$  transitions, as expected. In general, however,  $\sigma^{(7)}$  depends on the molecular alignment and it is sensitive to the ratio,  $|a_{\Pi}/a_{\Sigma}|$ , and relative phase,  $\delta_{\Pi-\Sigma}$ , of the amplitudes.

Note that the exact differential cross section for helium at equal sharing is given by  $|a_g|^2(\cos \theta_1 + \cos \theta_2)^2$ , with a single amplitude,  $a_g$ , that is often approximated by the Gaussian function:

$$|a_g|^2 \propto \exp[-4 \ln(2)(180 - \theta_{12})^2/\theta_{1/2}^2] \quad (2)$$

with the correlation half-width,  $\theta_{1/2}$ , depending solely on the excess energy,  $E = E_1 + E_2$ . This functional form gives remarkably accurate shapes for a wide range of  $E$ . The Gaussian ansatz has also been used in the analysis of previous studies in  $H_2/D_2$ . All these studies made restrictive hypothesis such as *real* amplitudes (i.e.,  $\delta_{\Pi-\Sigma} = 0, 180^\circ$ ) [2,14,15], or equal half-widths  $\theta_{1/2}$  for the  $\Sigma$  and  $\Pi$  amplitudes [14,15], or incorporated values of  $|a_{\Pi}/a_{\Sigma}|$  in conflict with Kossmann *et al.*’s [7] ion measurement [10] (see below).

In this work, still using the Gaussian ansatz, we were able to extract all four parameters as independent variables within a least squares fitting procedure. To this purpose the whole three-dimension  $E_1 = E_2$  coplanar data set has been considered, including all intermediate angular patterns comprised between Figs. 1 and 2 in steps of  $15^\circ$  in  $\theta_1$ , and the accepted solid angles of the experiment have been introduced in the fit. Our best fit values are  $|a_{\Pi}/a_{\Sigma}| = 2.25 \pm 0.35$ ,  $\theta_{1/2}^{\Pi} = 73^\circ \pm 2^\circ$ ,  $\theta_{1/2}^{\Sigma} = 93^\circ \pm 4^\circ$ , and  $\delta_{\Pi-\Sigma} = 70^\circ \pm 10^\circ$ . First, we find that it is impossible to obtain the observed *shapes* in the coplanar FDCS with a phase difference,  $\delta_{\Pi-\Sigma}$ , of  $180^\circ$ —the value obtained in all

the previous studies. Since  $\delta_{\Pi-\Sigma}$  is a function of the electron mutual angle  $\theta_{12}$ , the quoted value of  $70^\circ \pm 10^\circ$  should be seen as the average or effective phase difference. Second, at variance with recent calculations [2,10], we find that  $\theta_{1/2}^{\Sigma} > \theta_{1/2}^{\Pi}$  which is consistent with the observed variation of angular correlation between  $\Sigma$  and  $\Pi$  orientations in Figs. 1 and 2. Our width  $\theta_{1/2}^{\Pi} = 73^\circ \pm 2^\circ$  for the dominant  $\Pi$  component is significantly smaller than the width for helium at the same excess energy ( $90^\circ \pm 3^\circ$ ). Third, there is a connection, within Feagin’s formalism, between the  $|a_{\Pi}/a_{\Sigma}|$  value and the ion asymmetry parameter  $\beta_N$ , namely:

$$\beta_N = \frac{2(1 - |a_{\Pi}/a_{\Sigma}|^2)}{1 + 2|a_{\Pi}/a_{\Sigma}|^2}. \quad (3)$$

Our value  $|a_{\Pi}/a_{\Sigma}| = 2.25 \pm 0.35$  gives  $\beta_N \approx -0.73 \pm 0.1$ , which is fully compatible with previous ion measure-

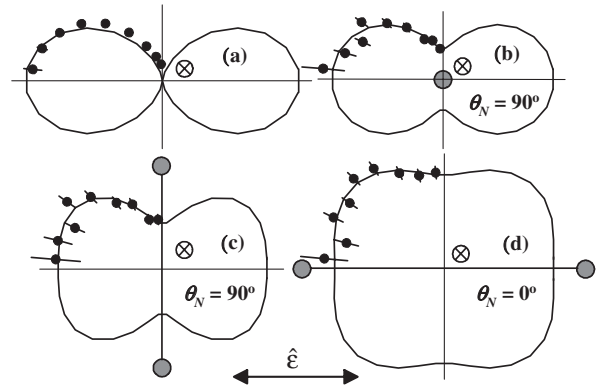


FIG. 3. Absolute FDCSs for  $H_2$  (b)–(d)—compared to that of helium (a)—for  $E_1 = E_2 = 12.5 \pm 2.5$  eV (a)–(c) and  $\pm 4$  eV (d), in the orthogonal geometry with first electron at  $\theta_1 = 90^\circ$ , perpendicular to the plane of the figure, which contains the second electron ( $|\phi_{12}| = 90^\circ$  or  $270^\circ$ ). The molecule is oriented (b) perpendicular to this plane ( $|\phi_{1N}| = 0^\circ$  or  $180^\circ$ ), and (c), (d) in this plane ( $|\phi_{1N}| = 90^\circ$  or  $270^\circ$ ). The four quadrants are related by symmetries (see text) and equivalent data have been added. The full lines are (a)  $(\cos \theta_2)^2$ ; (b)–(d) fits with partial waves up to  $\ell = 2$ , normalized to the data and the absolute scale is given by their maxima at 6 barns/eV/sr<sup>2</sup> (a) and 22 (b), 14 (c), 14 (d) millibarns/eV<sup>2</sup>/sr<sup>3</sup>. The angular bandwidths are  $\Delta \theta_1 = \pm 20^\circ$  (a)–(c),  $\pm 30^\circ$  (d);  $\Delta \phi_{12} = \pm 20^\circ$ ;  $\Delta \theta_N = \pm 25^\circ$  (b),(c),  $\pm 30^\circ$  (d);  $\Delta \phi_{1N} = \pm 45^\circ$ .

ments yielding  $\beta_N \approx -0.68 \pm 0.04$  for  $E = 25$  eV [7]. Analyzing the ions independently from the electrons in the present experiment leads to  $\beta_N \approx -0.75 \pm 0.1$ , also in good agreement with the above values.

In Fig. 3 a second subset of data, where  $\hat{k}_1$  is perpendicular to the plane containing  $\hat{k}_2, \hat{\varepsilon}$ , is reported. In this “orthogonal” geometry, first introduced in previous experiments [1], the electron-electron mutual angle,  $\theta_{12}$ , is a constant  $90^\circ$  and consequently the electron correlation aspect is “frozen,” in contrast with coplanar geometry. The  $H_2$  FDCSs for three different molecular orientations (b)–(d) and the corresponding results for helium (a) made under identical operating conditions are shown. Note that the FDCSs are in general much smaller than in Figs. 1 and 2. In the helium case, the shape of the FDCS is given exactly by  $\cos^2(\theta_2)$  and verified in our measurements [Fig. 3(a)]. For  $H_2$  the observed shapes of the FDCSs differ from  $\cos^2(\theta_2)$  and are all different from each other [Figs. 3(b)–3(d)], in contradiction with Eq. (1), which predicts a  $\cos^2(\theta_2)$  shape in all cases. These angular distributions are well reproduced by partial wave expansions up to  $\ell = 2$  (full lines on Fig. 3).

Clearly the orthogonal geometry reveals a significant inadequacy of the heliumlike model, whereas the coplanar FDCSs are strongly supportive. This is not so surprising as in the coplanar geometry the dominant physical effect, namely, the angular correlation, can be accounted for in the model through the two amplitudes. On the other hand, orthogonal geometry probes the so-called “kinematical factors” which reduce to the exact  $(\cos\theta_1 + \cos\theta_2)^2$  dependence in helium at equal energy sharing. The latter originates in angular momentum conservation in the atomic case, and in the  $P$  character of the outgoing electron pair. However, in the molecular case only the projection of angular momentum onto the nuclear axis is conserved, and the outgoing pair may have higher angular momentum and may not have axial symmetry around the  $\hat{\varepsilon}_\Pi$  component, as assumed in Feagin’s derivation. Therefore, it is likely that the already mentioned exact approach [13] using generalized shape coordinates for the  $H_2$  system could shed some light on the present observations, by allowing one to in-

vestigate terms that go beyond the first order. In addition, there is currently much effort in applying time-dependent close coupling (TDCC) [16], exterior complex scaling (ECS) [6,17] methods to this problem, both of which have been successful in helium. Our extensive data set will allow a direct comparison with such methods in the near future.

In summary, the reported analysis, restricted to equal energy sharing, has been focused on the effect of molecular orientation, from pure  $\Pi$  to pure  $\Sigma$ , on the electron angular distributions. Further investigation, including unequal energy sharing and other dynamical effects—such as the role of the internuclear separation—is in progress and will be the object of forthcoming publications.

We would like to thank the staff at Elettra and the Gas Phase beam line team for their invaluable assistance, and EU, NSERC, and UoW for their financial support.

- 
- [1] T. Weber *et al.*, *Nature (London)* **431**, 437 (2004).
  - [2] T. Weber *et al.*, *Phys. Rev. Lett.* **92**, 163001 (2004).
  - [3] M. Gisselbrecht *et al.*, *Rev. Sci. Instrum.* **76**, 013105 (2005).
  - [4] M. Lavollée, *Rev. Sci. Instrum.* **70**, 2968 (1999).
  - [5] H. Bräuning *et al.*, *J. Phys. B* **31**, 5149 (1998).
  - [6] W. Vanroose *et al.* *Phys. Rev. A* **70**, 050703(R) (2004).
  - [7] H. Kossmann *et al.*, *Phys. Rev. Lett.* **63**, 2040 (1989).
  - [8] J. M. Feagin, *J. Phys. B* **31**, L729 (1998).
  - [9] T. J. Reddish and J. M. Feagin, *J. Phys. B* **32**, 2473 (1999).
  - [10] A. S. Kheifets, *Phys. Rev. A* **71**, 022704 (2005).
  - [11] A. S. Kheifets and I. Bray, *Phys. Rev. A* **72**, 022703 (2005).
  - [12] M. Walter and J. S. Briggs, *Phys. Rev. Lett.* **85**, 1630 (2000).
  - [13] M. Walter, A. Meremianin, and J. S. Briggs, *J. Phys. B* **36**, 4561 (2003).
  - [14] J. P. Wightman, S. Cvejanović, and T. J. Reddish, *J. Phys. B* **31**, 1753 (1998).
  - [15] N. Scherer, H. Lörch, and V. Schmidt, *J. Phys. B* **31**, L817 (1998).
  - [16] J. Colgan, M. S. Pindzola, and F. Robicheaux, *J. Phys. B* **37**, L377 (2004).
  - [17] W. Vanroose *et al.*, *Science* **310**, 1787 (2005).